Received: 18 June 2021 | Revised: 3 August 2021 | Accepted: 30 August 2021

DOI: 10.1111/cbdd.13948

RESEARCH ARTICLE

WILEY

Glucosyl-1,2,3-triazoles derived from eugenol and analogues: Synthesis, anti-*Candida* activity, and molecular modeling studies in CYP-51

Lorena Severiano de Magalhães[1] | **Adriana Cotta Cardoso Reis**[1] | **Izadora Amaral Nakao**[1] | **Vinícius Augusto Campos Péret**[1] | **Rúbia Castro Fernandes Melo Reis**[1] | **Naiara Chaves Silva**[2] | **Amanda Latércia Tranches Dias**[2] | **Diogo Teixeira Carvalho**[3] | **Danielle Ferreira Dias**[4] | **Geraldo Célio Brandão**[1] | **Saulo Fehelberg Pinto Braga**[1] | **Thiago Belarmino de Souza**[1]

[1]School of Pharmacy, Federal University of Ouro Preto, Ouro Preto, Brazil

[2]Institute of Biomedical Sciences, Federal University of Alfenas, Alfenas, Brazil

[3]Pharmaceutical Sciences University, Federal University of Alfenas, Alfenas, Brazil

[4]Institute of Chemistry, Federal University of Alfenas, Alfenas, Brazil

Correspondence
Thiago Belarmino de Souza, School of Pharmacy, Federal University of Ouro Preto, Ouro Preto, Brazil.
Email: thiagobs83@yahoo.com.br

Funding information
Fundação de Amparo à Pesquisa do Estado de Minas Gerais; Conselho Nacional de Desenvolvimento Científico e Tecnológico

Abstract

This work describes the synthesis, anti-*Candida*, and molecular modeling studies of eighteen new glucosyl-1,2,3-triazoles derived from eugenol and correlated phenols. The new compounds were characterized by combined Fourier Transform Infrared, ^{1}H and ^{13}C nuclear magnetic resonance and spectroscopy of high-resolution mass spectrometry. The synthesized compounds did not show significant cytotoxicity against healthy fibroblast human cells (MCR-5) providing interesting selectivity indexes (SI) to active compounds. Considering the antifungal activity, nine compounds showed anti-*Candida* potential and the peracetylated triazoles 17 and 18 were the most promising ones. Eugenol derivative 17 was active against three species of *Candida* at 26.1–52.1 μM. This compound was four times more potent than fluconazole against *Candida krusei* and less toxic (SI > 6.6) against the MCR-5 cells than fluconazole (SI > 3.3) considering this strain. Dihydroeugenol derivative 18 showed similar activity to 17 and was four times more potent and less toxic than fluconazole against *C. krusei*. The deacetylated glucosides and non-glucosylated corresponding derivatives did not show considerable antifungal action, suggesting that the acetyl groups are essential for their anti-*Candida* activity. Molecular docking coupled with molecular dynamics showed that 14α-lanosterol demethylase is a feasible molecular target, since 17 and 18 could bind to this enzyme once deacetylated *in vivo*, thereby acting as prodrugs. Also, these studies demonstrated the importance of hydrophobic substituents at the phenyl ring.

KEYWORDS

anti-*Candida* activity, CYP51, eugenol, glycosyl-triazoles, molecular docking, molecular dynamics

1 | INTRODUCTION

Indicators of morbidity and mortality from fungal infections are increasing at an alarming rate, both in immunocompetent and in immunosuppressed patients. It is estimated that there are approximately six million fungal species in the world and about 600 species can cause diseases in humans. These infections affect over one billion people each year and leading to more than 1.5 million deaths worldwide annually (Strickland & Shi, 2021).

Candida infection is one of the most common fungal infections and *Candida albicans* is the most commonly recovered from clinical species, followed by *Candida glabrata*. Other clinically important species include *C. parapsilosis*, *C. krusei*, *C. tropicalis*, *C. dubliniensis*, *C. lusitaniae*, and the most recent, *C. auris*. *C. auris* is an emerging multiresistant species that is difficult to diagnose and is causing great concern in health centers currently. The cases associated with *C. auris* increased by 318% between 2015 and 2018 (Bhattacharya et al., 2020). In Latin America, these infections are caused mainly by *C. albicans*, but other species are also relevant and prevalent under certain conditions. For example, vulvovaginal candidiasis in diabetic patients and patients with hematological diseases is often caused by *C. glabrata*. Patients undergoing treatment for myeloid leukemia commonly present infection by *C. tropicalis*. Invasive infections by *C. krusei* are very relevant in bone marrow transplant patients. *C. parapsilosis* causes infections mainly in children and is the second leading cause of endocarditis (Whaley et al., 2017).

There are only three classes of available drugs for the treatment of systemic fungal infections, the polyene amphotericin B, echinocandins and azoles. Most species of fungi have already developed resistance to these drugs and, in addition to resistance problems, these drugs can lead to adverse effects as nausea and vomiting, besides some potentially dangerous effects, such as liver and kidney toxicity, and hepatobiliary disorders (Revie et al., 2018).

Lately, our research group has spared no efforts in the search of new substances with antimicrobial potential that can increase the therapeutic arsenal for the treatment of these infections. We have focused mainly on the synthesis of glycosidic derivatives of eugenol (**I**, Figure 1), a natural allylphenol that shows several biological activities, including antifungal. Linking bioactive compounds to carbohydrate residues (as glucose) could increase the ability of these compounds to penetrate microorganism cells through glucose transporters present in fungal membranes and contribute to modulate important physicochemical properties for drug action, such as solubility. Furthermore, the insertion of saccharide units in a bioactive substance can lead to an increase in its biological activity by creating new points of attachment with a target of the microorganism. Therefore, we recently reported the synthesis of eugenol glucosides with antifungal potential: Derivative **II** was active against *Candida glabrata* at 3.4 μM (3.4 times more potent than fluconazole), and derivative **III** showed fungistatic (IC_{50}: 18.1 μM) and fungicidal (IC_{50}: 36.2 μM) activities against this same strain (Souza et al., 2014, 2016).

Based on the anti-*Candida* activity observed for glycosidic derivatives **II** and **III**, we report herein the synthesis and evaluation of new glucosyl triazoles derivatives of eugenol and related substances (dihydroeugenol, guaiacol, phenol, vanillin, and isoeugenol) with the structural pattern showed in Figure 2. In addition to the glucosylated compounds (in peracetylated and deacetylated forms), the respective non-glucosylated derivatives were also synthesized to evaluate the importance of the saccharide moiety in the antifungal activity. We decided to associate the saccharide unit to the phenols through a 1,2,3-triazole ring from a click reaction, which is already a well-established reaction by our research group. This heterocycle could

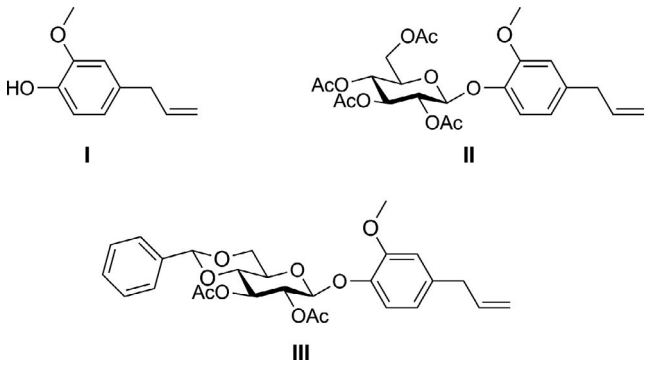

FIGURE 1 Eugenol (**I**) and glucosyl derivatives (**II** and **III**) with antifungal activity

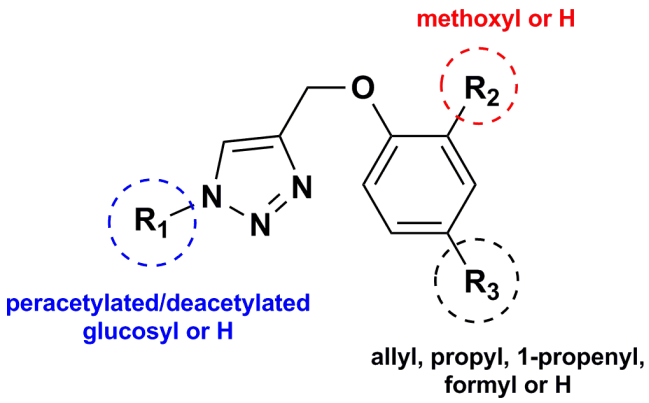

FIGURE 2 Structural pattern of glucosylated and non-glucosylated 1,2,3-triazoles derived from eugenol and analogues

also act as an isoster of pharmacophore azole rings present in different drugs as ketoconazole, miconazole, and other antifungal agents, and here, we could evaluate the influence of this group in the mono or disubstituted form regarding its potential to mimic different azole rings of these drugs. Moreover, with the proposed compounds, we were able to have a greater understanding about the importance of carbohydrate and the groups from eugenol to their antifungal potential against *Candida* spp.

2 | RESULTS AND DISCUSSION

2.1 | Chemistry

The new triazoles derived from eugenol and analogues were synthesized according to the synthetic route seen in Scheme 1.

First, eugenol (**1**) and the other phenols (**2**–**6**) were alkylated from the Williamson synthesis, using propargyl chloride to provide the alkynes **7**–**12** by the method described by Achard et al. (2011). In parallel, D-glucose (**13**) was converted to its peracetylated derivative (**14**) after its reaction with acetic anhydride, which subsequently provided the acetobromoglucoside (**15**) after reaction with hydrobromic acid and acetic acid (Guilherme et al., 2019). The reaction of **15** with sodium azide led to the α-glucosyl azide **16,** which was employed in the next step without previous purification (Pote et al., 2018). The reaction of alkynes (**7**–**12**) with the glucosyl azide **16** by cooper catalyzed 1,3-dipolar cycloaddition ("click" reaction) resulted in the peracetylated 1,2,3-triazole derivatives (**17**–**22**) with yields in the range of 51–71%. Copper (I) acts by complexing with the terminal carbon of the alkyne generating a metal acetylide and the nucleophilic nitrogen of the alkylazide attacks the complexed copper, directing the formation of the 1,4-regioisomer (Safavi et al., 2019). The deacetylated 1,2,3-triazoles (**23**–**28**) were obtained with yields in the range of 30–98% after methanolysis of glucosides **17**–**22** (Safavi et al., 2019). In order to evaluate the importance of the saccharide unit in the structure of the compounds, the respective non-glycosylated triazoles (**29**–**34**) were also synthesized from the reaction of the alkynes **7**–**12** with sodium azide and acetic acid, thus obtaining yields in the range of 57–61% (Banert et al., 2016).

The analysis of infrared spectra of derivatives **17**–**22** showed typical bands of ester carbonyl and aromatic C=C stretching near 1740 and 1599–1450 cm^{-1}, respectively. For deacetylated triazoles **23**–**28**, hydroxyl bands near 3300 cm^{-1} were noticed as expected. In ^{1}H nuclear

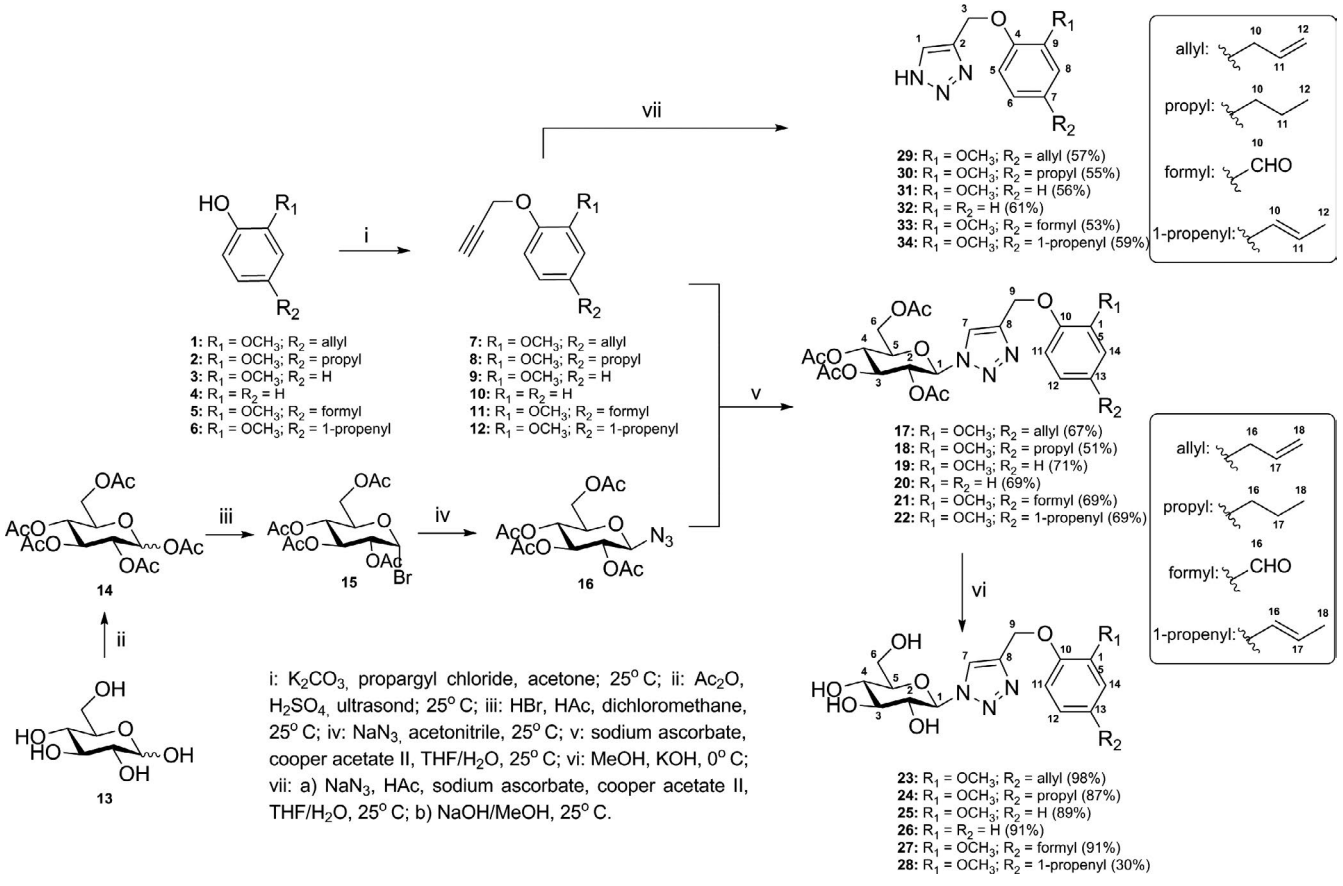

SCHEME 1 Synthesis of glucosylated-1,2,3-triazole derivatives of eugenol and analogues

magnetic resonance (NMR) spectra of derivatives **17**–**22**, a singlet was registered near 7.40 ppm corresponding to the 1,2,3-triazolic ring proton, proving the formation of this heterocycle. The signals related to the aromatic hydrogens were recorded between 7.0 and 6.6 ppm, according to the substitution pattern of each compound. The saccharide hydrogens were observed between 6.38 and 3.95 ppm, while the acetyl group hydrogens were recorded as singlets between 2.91 and 2.18 ppm. For deacetylated derivatives **23**–**28**, singlets and triplets referring to hydroxyl groups were observed, with coupling constants between 5 and 6 Hz. A typical trans-diaxial coupling constant (^3J 8.0 Hz) was observed for the anomeric hydrogen of all final glucosides, which confirms that all of them were obtained as the β-anomers. In the ^{13}C NMR spectra of derivatives **17**–**22**, signals between 170.6 and 168.0 ppm corresponding to the ester carbonyl groups were observed. The signals of the saccharide carbons were recorded between 85 and 63 ppm for all the glucosides. The methylene carbon attached to the triazolic ring gave a signal near 70 ppm for triazoles **17**–**28** and near 62 ppm for triazoles **29**–**34**. The infrared and NMR spectra of all synthesized compounds are presented in the Supplementary Material.

The synthesized 1,2,3-triazoles were also characterized by high-resolution mass spectrometry (HRMS), and the molecular ion peak values are shown in Table A (Supplementary Material) As could be observed, the mass accuracy between the calculated and found values was lower than 5 ppm, which are acceptable for proposing a molecular formula using this technique (Balogh, 2004). The HRMS spectra are also presented in the Supplementary Material.

Other physicochemical properties of 1,2,3-triazoles **17**–**34** were determined (solubility and calculated logP) in order to have a better understanding of the biological results described below. These data are shown in Table B (Supplementary Material).

2.2 | Biological assays

Following, the compounds were evaluated against different species of fungi (*Candida albicans*, *C. tropicalis*, *C. krusei*, *C. glabrata*, and *C. parapsilosis*) by the microdilution method, and the results were estimated using the inhibitory concentration that was able to inhibit 50% of microbial growth (IC_{50}; fungistatic activity; EUCAST - European Committee on Antibiotic Susceptibility Testing, 2008). The cytotoxicity of the compounds was also evaluated against healthy human lung fibroblast cells (MRC-5 cells) by MTT colorimetric method (Mosmann, 1983; Twentyman & Luscombe, 1987). The selectivity indexes (SI) were determined by the ratio CC_{50} (MRC-5)/IC_{50} of each strain. The results are shown in Table 1.

The synthesized compounds did not show significant cytotoxicity against fibroblast human cells (MCR-5), with CC_{50} values varying between 173.8 and 487.6 μM, which was sufficient to confer interesting SI values for the active substances. Considering the antifungal activity, the peracetylated triazoles **17** (derived from eugenol) and **18** (derived from dihydroeugenol) were the most promising ones. Triazole **17** was active against three species of *Candida* (*C. tropicalis*, *C. krusei*, and *C. glabrata*) with IC_{50} values in the range 26.1–52.1 μM. This compound was four times more potent than fluconazole against *C. krusei*, presenting a good selectivity to this species, although it was not active against *C. albicans* or *C. parapsilosis*. In addition, triazole **17** was less toxic against the MCR-5 cells (SI > 6.6) than fluconazole (SI > 3.3) considering *C. krusei*. The compound **18** showed considerable activity against *C. tropicalis* e *C. krusei*, as observed for its analogue **17**. This compound was four times more potent and less toxic than fluconazole against *C. krusei* and as active as **17** against *C. tropicalis* with the same IC_{50} value (25.98 μM). The prominent antifungal activity and spectrum of action found by the derivatives **17** and **18** suggest that the presence of acetyl groups contributed positively to anti-*Candida* activity, since the respective deacetylated glycosides (**23** and **24**) did not show considerable antifungal action. The peracetylated triazoles **19**, **20**, **21**, and **22** were inactive against the evaluated strains. This allows us to conclude that the presence of an allyl or propyl chain seems to cooperate significantly to antifungal activity, as seen in the compounds **17** and **18**. The conjugation of a double bond with the aromatic ring also appears to be deleterious for the antifungal activity of the compounds, since derivatives **21** (formyl group conjugated) and **22** (1-propenyl group conjugated) were also inactive. Another important observation about the structure–activity relationship of the synthesized substances is that the presence of carbohydrate is essential for anti-*Candida* activity, since the non-glycosylated derivatives corresponding to **17** and **18** (**29** and **30**, respectively) were inactive or weakly active against some species (IC_{50} values between 242.7 and 407.9 μM). Finally, when comparing the anti-*Candida* activity of glucosyltriazoles **17** and **18** with the peracetylated glycoside of eugenol already reported by our group (compound **II**, Figure 1), we can conclude that the presence of the 1,2,3-triazole ring contributed to a large increase in activity against *C. tropicalis* and *C. krusei*, as related triazoles were active at 26.1 μM against these two strain, while glycoside **II** was weakly active at 202 μM.

TABLE 1 *In vitro* antifungal activity (IC_{50}, μM), cytotoxicity against MRC-5 cells (CC_{50}, μM) and selectivity index (SI, CC_{50}/IC_{50}) of the compounds **17**–**34**

Compound	*Ca* (SI) IC_{50}	*Ct* (SI) IC_{50}	*Ck* (SI) IC_{50}	*Cg* (SI) IC_{50}	*Cp* (SI) IC_{50}	*MRC-5* CC_{50}
17	–[a]	26.1 (>6.6)	26.1 (>6.6)	52.1 (>3.3)	–	>173.8
18	173.2 (>1)	25.98 (>6.7)	25.98 (>6.7)	103.94 (>1.6)	–	>173.2
19	–	–	–	–	–	>186.8
20	–	–	–	–	–	>197.95
21	–	–	–	–	–	>177.5
22	–	–	173.8 (>1)	–	–	>173.8
23	245.6 (>1)	–	245.6 (>1)	–	245.6 (>1)	>245.6
24	244.3 (>1)	–	–	–	–	>244.3
25	–	–	–	–	–	158.7 ± 1.63
26	–	–	–	–	–	>296.6
27	–	–	–	–	–	>253.1
28	–	–	147.3 (>1.6)	–	–	>245.6
29	–	–	407.98 (0.52)	–	–	215.6 ± 2.19
30	404.6 (0.65)	–	–	404.6 (0.65)	242.7 (1.1)	265.8 ± 1.33
31	–	–	–	–	–	>487.6
32	–	–	–	–	–	–
33	–	–	–	–	–	>429.0
34	–	–	407.9 (0.4)	407.9 (0.4)	–	180.4 ± 1.53
Fluconazole	3.2 (>102)	3.2 (>102)	104.4 (>3.1)	16 (>20)	6.4 (>51)	>326.5

[a]Inactive at highest evaluated concentration; *Ca*: *Candida albicans* ATCC 10231; *Ct*: *Candida tropicalis* ATCC 750; *Ck*: *Candida krusei* ATCC 6258; *Cg*: *Candida glabrata* ATCC 90030; *Cp*: *Candida parapsilosis* ATCC 22019; and MRC-5: human lung fibroblasts cells.

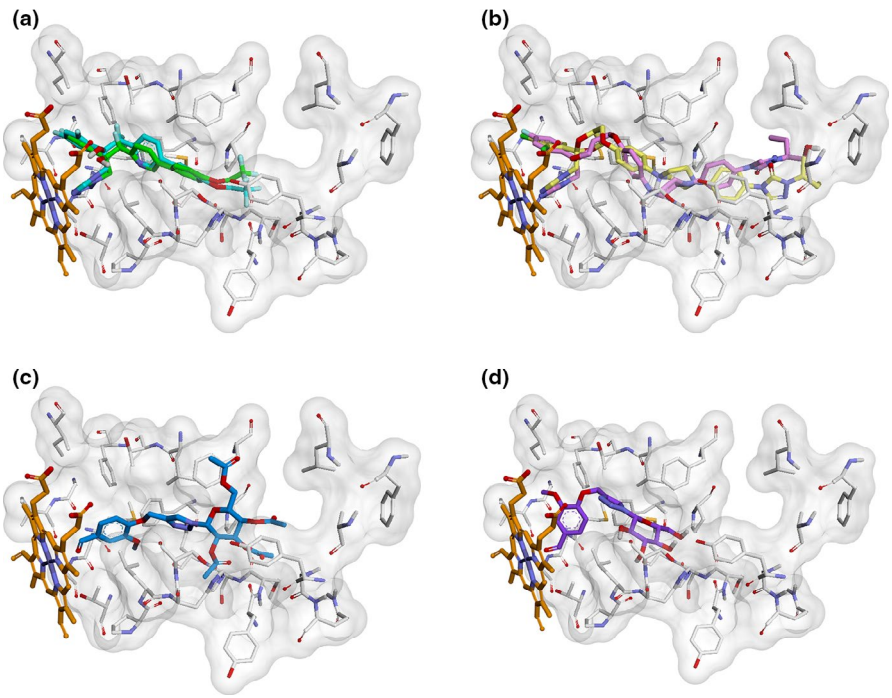

FIGURE 3 (a) Comparison between lowest RMSD solution of **VT1** from redocking (cyan sticks) and its crystallographic conformation (green sticks). (b) Best docking solutions of **itraconazole** (yellow sticks) and **posaconazole** (pink sticks). (c) Best docking solution of peracetylated compound **21** (blue sticks). (d) Best docking solution of deacetylated compound **27** (purple sticks). The heme prosthetic group is shown in orange sticks, and some binding site residues are shown as white sticks with a transparent solvent accessible surface

2.3 | Molecular modeling studies

In order to investigate the likely mechanism of action of the active derivatives, we decided to perform docking studies of the synthesized compounds on 14α-lanosterol demethylase (CYP51). This is a heme-containing enzyme that is involved in ergosterol synthesis, hence vital for membrane stability and fungal survival. It is one of the most explored targets for fungi and has as representative approved drugs itraconazole, posaconazole, and fluconazole (Mani Chandrika & Sharma, 2020). Given the presence of an azole and an aromatic ring in their structures, the synthesized compounds in this study bear some structural similarity with marketed inhibitors of CYP51. It is known from crystallographic structures that this azole ring establishes an important interaction with the iron in the heme cofactor, and this is the reason why it is considered the pharmacophore of the azole drugs (Hargrove et al., 2017; Peyton et al., 2015). By performing docking of the triazole derivatives against CYP51, we sought to investigate not only the probability of acting on this target, but also the role of the triazole ring in the predicted complex.

The crystallographic structure used in the molecular modeling studies (PDB code 5tz1) consisted of a 14α-lanosterol demethylase from *C. albicans*, one of the evaluated species, and it was resolved in an adequate resolution of 2.0 Å. The structure is a complex of the protein with the inhibitor **VT1**, also an azole compound, in which, it is possible to observe a coordination between a nitrogen from the azole ring and the iron atom from the heme group (Hargrove et al., 2017).

The docking protocol was determined by choosing a scoring function, the number of runs, and size of the search area that reproduced the ligand conformation closer to the crystallographic complex, given by its root mean square deviation (RMSD). The value found of 1.03 Å was lower than the 2.0–2.5 Å usually recommended in the literature, thus confirming the protocol liability in predict ligand conformation (Figure 3a). More importantly, the docking correctly predicted the azole-iron coordination found in the crystallographic structure.

For referencing purposes, two known azoles that act in the CYP51 system were also docked: itraconazole and posaconazole. Both drugs had the same binding mode of **VT1**: one nitrogen of the azole ring interacting with the iron atom in the heme group, a hydrogen bond with a conserved water and the halide substituted phenyl ring inserted into a hydrophobic pocket near the heme group (Figure 3b). Additionally, their protonated piperazine ring is capable of establishing an additional hydrogen bond with a conserved water molecule. Altogether, these observations illustrate the importance of the azole ring and help to explain the higher Goldscore obtained in the docking experiment (**VT1** 91.8 vs **itraconazole** 117.9 and **posaconazole** 105.7).

When analyzing synthesized 1,2,3-triazoles **17**–**34**, the top3 ranked compounds, with a Goldscore close to **VT1**'s, were peracetylated compounds (**17**, **18**, and **21**). In the predicted binding poses, the carbohydrate moiety is placed near the entrance of the binding site, while the phenyl ring is pointed toward the heme group. Interestingly, the carbonylic oxygens of compound **21** found 2.63 Å away from the heme iron atom, thereby establishing an interaction (Figure 3c). Although the deacetylated derivatives ranked more inferiorly classified than the peracetylated, hence removal of acetyl groups allowed the molecule to position itself deeper into the pocket, as observed by a shift of 3.49 Å when comparing **27** and **21** glucosidic rings (Figure 3d). Also, some of the free hydroxyls could engage hydrogen bond with a conserved water in the binding site, as seen in predicted binding poses of the approved drugs and the phenyl ring is positioned deeper in the pocket, establishing hydrophobic contacts. Although these hydrogen bonds contributed to their final scoring, peracetylated larger van der Waals contribution and water displacement were more relevant, as the binding pocket is formed mostly by hydrophobic residues. However, deacetylated derivatives might play an important role in antifungal activity, since the peracetylated compounds could be metabolized once absorbed by fungi to desacetylated corresponding derivatives.

Despite their lower Goldscore (<63.69), monosubstituted triazoles **29** and **30** had a similar interaction mode than azole drugs regarding the heme group. The low score and antifungal activity shown by these non-glycosylated derivatives could be associated with their lower molecular weight, as less atoms are available to interact with the target; therefore, further optimization should be considered to try to improve their action. For instance, compound **30** had a discreet activity against *C. parapsilosis* and it has a reasonable logP for improved cellular penetration (calculated logP 2.62).

Since docking has some intrinsic limitations, such as treating the protein as a rigid body and the absence of an explicit water model, molecular dynamics (MD) were performed in order to refine docking results and observe the binding dynamics. Since this method has a higher computational cost when compared to docking, we choose representative molecules for this study: the crystallographic ligand (**VT1**), the best ranked peracetylated (**21**) and deacetylated (**27**), the best-monosubstituted triazole (**30**), the most active compound (**18**) and its deacetylated derivative (**24**). We also decided to include an inactive compound in the studies. For this purpose, we searched the ChEMBL database for inactive compounds tested against *C. albicans* 14α-lanosterol demethylase and selected

compound **13758** for being more structurally related to synthesized compounds (Figure 4).

The complex stability was confirmed during the equilibration phase by monitoring the fluctuation of the temperature, pressure, and density of the system. Also, in all complexes, the protein radius of gyration (Rg), an indication of protein compactness, was maintained stable during the entire 20 ns production simulation and a similar RMSF profile was observed for all complexes (Figure 5; Lemkul, 2019).

The protein in all the complexes had only small conformation changes throughout the simulation, given by their mean heavy atoms RMSD (1.5–1.9 Å) to the crystallographic structure. These changes occurred mostly at the beginning of the simulation, since the complex is going from a crystal packing to a solvated system.

As for the ligands, when compared to the initial conformation from docking, **VT1** and **30** had the least variation, with a mean RMSD below 2.0 Å, while compound **24** had an acceptable variation (2.5 Å). In the contrary, compounds **18**, **21**, and **27**, as well as the inactive compound **13758**, had significative variations in their conformations during the trajectory indicating that docking failed to correctly predict these complex conformations, resulting in non-stable ones (Figure 5f).

Although ligands with hydrophobic character are welcome in this particular binding site, it seems reasonable to think that extra volume conferred by acetyl groups of peracetylated compounds might be the cause of such conformation changes. When comparing the trajectories of peracetylated compound **18** and its correspondent deacetylated **24**, there is a clear difference in the binding dynamics. While **18** moves outwards of the hydrophobic channel, thus leaving the binding pocket, compound **24** has a lateral movement, placing its phenyl ring deeper in the hydrophobic pocket near heme-binding site (Figure 6).

Although peracetylated compounds **17** and **18** performed better than correspondent deacetylated in the *in vitro* assays, the possibility of these compounds act as prodrugs might help to explain such divergence. It is known that ester groups could be readily hydrolyzed once inside fungal cells, thus affording deacetylated compounds which in turn can bind to the molecular target in the cytoplasmic side of plasma membrane (Monk et al., 2014). Consequently, compounds **17** (logP: 3.34) and **18** (logP: 3.25), having a presumably better absorption profile given by their calculated logP, would penetrate the fungal to afford their correspondent deacetylated active compounds. On the other side, when tested directly, deacetylated **23** (logP: 0.53) and **24** (logP: 0.61) are too much hydrophilic to cross the fungal membrane, being inactive in the *in vitro* assays.

As coordination between azole ring and the heme iron atom is an important feature in ligand binding, we also

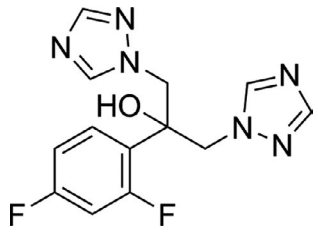

FIGURE 4 Structure of inactive compound **13758**

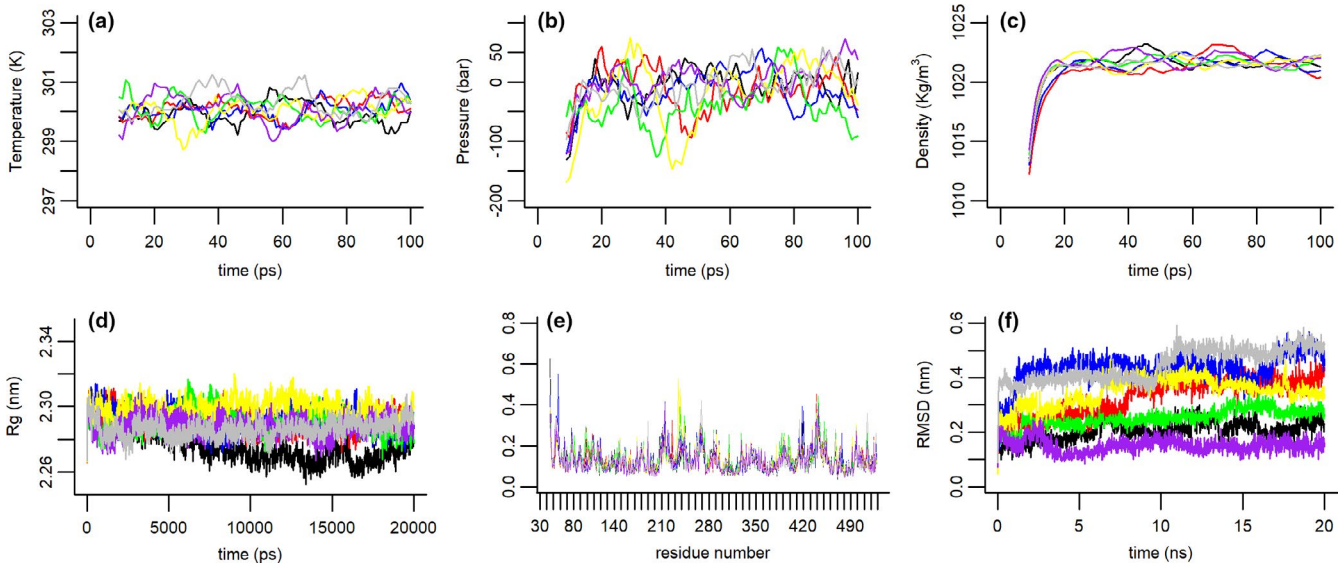

FIGURE 5 10ps moving averages of parameters monitored during the equilibration phase: temperature (a), pressure (b), and density (c); and the protein radius of gyration in the MD simulation (d). **VT1** (black), **17** (red), **21** (blue), **24** (green), **27** (yellow), **30** (purple), and **13758** (gray)

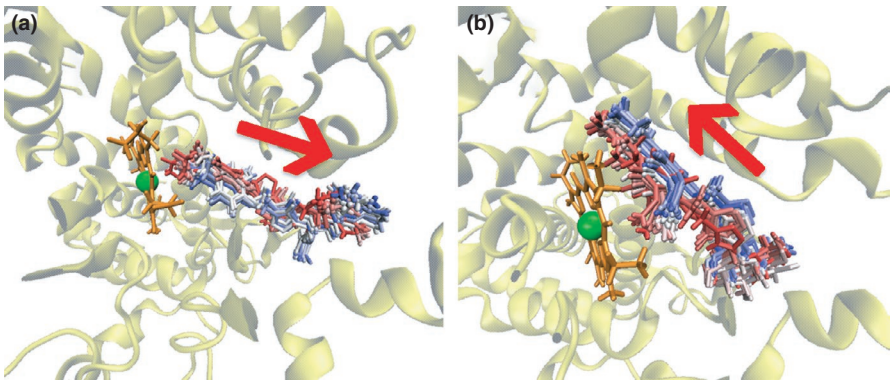

FIGURE 6 Trajectory snapshots of **18** (a) and **24** (b). The snapshots were extracted at each 1 ns of simulation and the ligand gradient colored from red (first frame) to blue (last frame). A referencing protein is partially shown as a yellow ribbon and the heme group as orange sticks with the iron atom highlighted as a green sphere. The arrow indicates the tendency of the ligand movement in the binding site

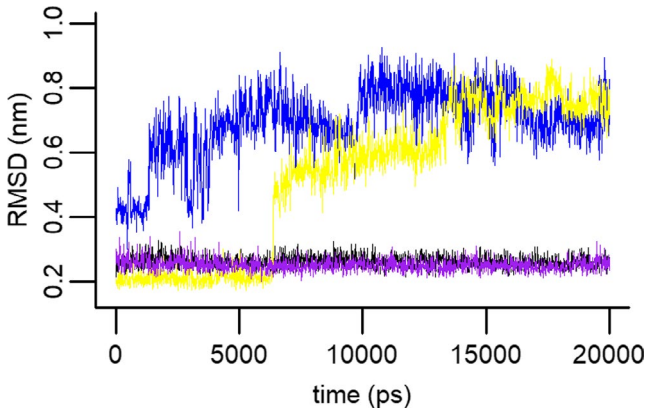

FIGURE 7 Interatomic distance between triazole nitrogen (**VT1** and **30**) or carbonylic oxygen (**21** and **27**) and the iron atom throughout the simulation. **VT1** (black), **21** (blue), **27** (yellow), and **30** (purple)

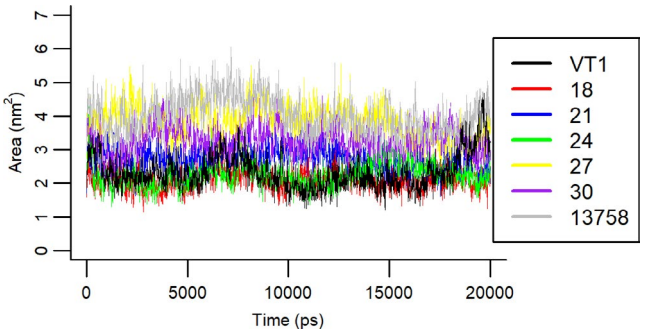

FIGURE 8 Solvent-accessible surface area of binding site residues throughout the simulation

measured the distance between ligand triazole nitrogen and the iron throughout the simulation (Hargrove et al., 2017; Lepesheva et al., 2018; Lepesheva & Waterman, 2004). Both **VT1** and **30** maintained a mean distance between these atoms compatible with a coordination bond (**VT1** N-Fe: 2.6 Å and **30** N-Fe: 2.5 Å; Figure 7; Kirton et al., 2005). As for the other ligands, the phenyl ring was turned toward the heme group while the triazole ring was too far away to establish any interaction. Though **21** and **27** could engage such interaction *via* their carbonylic oxygen, only in the complex with **27** this interaction was observed, although only in the first 5 ns, when a significant conformational change occurred (Figure 7).

The solvent-accessible surface area (SASA) is an important measure when analyzing ligand binding and complex stability. A relatively lower SASA means a greater complementarity between ligand and the biding site and a large difference between SASA in the bounded and nonbonded complex could indicate the displacement of water molecules in the binding site (Alonso et al., 2006). For reference, the residues of the binding site in the **VT1** complex had a mean SASA of 2.33 nm^2, while **18** and **21** had a SASA of 2.11 and 2.73 nm^2, respectively (Figure 8). The complex with compound **24** had a SASA of 2.26 nm^2, close to the crystallographic ligand, despite its lower molecular weight (Figure 8). In CYP51, a binding site which is formed mostly by hydrophobic residues, where the displacement of highly organized water could favor complex formation by a gain in the system entropy (Alonso et al., 2006). On the other side, the complexes with compounds **27** and **30** had a calculated SASA closer to complex with the inactive compound **13758** (3.81, 3.27, and 4.00 nm^2, respectively), meaning that the binding site is not effectively occupied by these ligands (Figure 8).

The total interaction energy of the complex calculated by Gromacs (sum of Coulombic and Lennard-Jones terms) could provide an estimate of complex affinity, although other parameters should be considered to determine the ligand binding energy, such as the solvation effects. Considering the last 15 ns of simulation, most compounds had a total interaction energy close to **VT1**

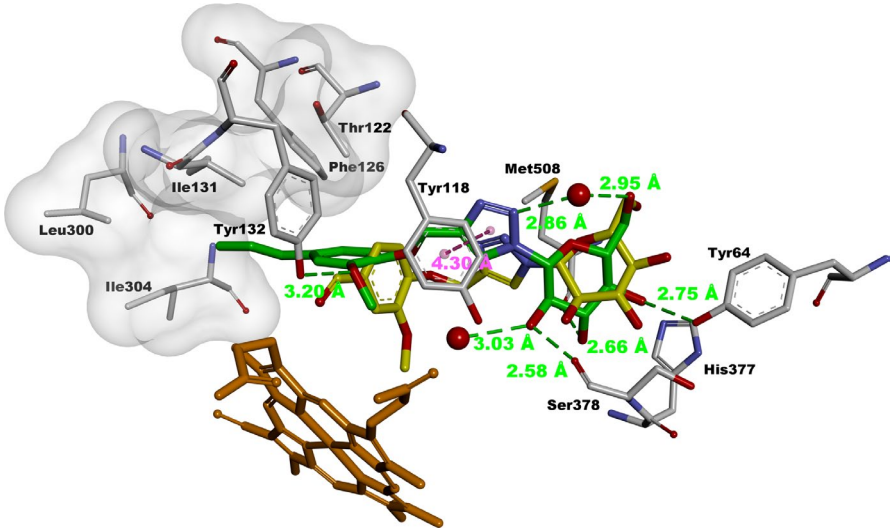

FIGURE 9 Representative conformations of **24** (green sticks) and **27** (yellow sticks) extracted from final 1ns of MD after clustering. The heme prosthetic group is shown in orange sticks; water molecule oxygens are shown as red-scaled balls and important binding site residues as white sticks. Only the main non-bonding interactions between CYP51-**24** are shown as dashed lines (green, hydrogen bond; pink, π-stacking) and distances in angstroms for clarity. A solvent-accessible surface was of residues Thr122, Phe126, Ile131, Leu300, and Ile304 is shown to emphasize the hydrophobic pocket

(−299.06 kcal/mol), while the inactive **13758** and **30** had the worst interaction energy (−184.09 and −173.28 kcal/mol, respectively). Surprisingly, compound **24** had an IE of −390.96 kcal/mol, value 30% lower than **VT1**, indicating a greater affinity.

Visualization of both trajectories reveals that propyl (**24**) and carbonyl (**27**) groups end up in a hydrophobic pocket formed by residues Thr122, Phe126, Ile131, Leu300, and Ile304 (Figure 9). As this pocket surrounds heme carboxylates, repulsion with the carbonylic oxygen of **27** might be the cause of positive coulombic component in the complex. When analyzing each term of the interaction energy separately, the major contribution interaction energy of **24** with aforementioned residues comes from the Lennard-Jones, while the Coulombic term is close to zero, meaning a strong hydrophobic contribution to the interaction energy. In relation to **27**, the Coulombic contribution is larger at first and turns repulsive at the end of simulation, due to proximity to heme carboxylates. Also, the calculated SASA of these residues for complex with **24** has the same value of **VT1** (0.12 nm^2), while in the complex with **27** the SASA is more than doubled (0.28 nm^2).

In Figure 9 is also possible to visualize the main nonbonded interactions between **24** and the protein. In addition to those arising from insertion of propyl substituent in the hydrophobic pocket, a π-stacking interaction is observed between triazole ring and the Tyr118 residue. Several hydrogen bonds were also observed, mainly from saccharidic portion, with some of them involving water molecules. Interesting, the oxygen in the methoxy group acts as a hydrogen bond donor in the interaction with Tyr132. A similar interaction is observed with VT1 and in other crystallographic complexes (i.e., 5EAD and 5ESM), but with the alcoholic hydroxyl and mediated by water.

3 | CONCLUSION

In this research study, eighteen new glucosyl-1,2,3-triazoles derived from eugenol and analogues were synthesized and characterized by spectroscopy and spectrometry methods. The new compounds were evaluated against *Candida* spp. by microdilution method, and the promising ones were peracetylated derivatives **17** (an eugenol derivative) and **18** (a dihydroeugenol derivative). Furthermore, the triazole **17** was active *C. tropicalis*, *C. krusei*, and *C. glabrata* at 26.1–52.1 μM, and it was four times more potent than fluconazole against *C. krusei*. Derivative **18** showed a wider spectrum of activity than **17**, and it was four times more potent and less toxic than fluconazole against *C. krusei* and as active as **17** against *C. tropicalis*. Altogether, molecular modeling studies suggest that antifungal activity of compounds **17** and **18** might be due to inhibition of CYP51, thereby disrupting fungal ergosterol synthesis. Since their respective deacetylated derivatives, **23** and **24,** showed to be more promising but had lower activity *in vitro*, we believe that peracetylated compounds might be acting as prodrugs. Guided by the molecular modeling results, further modifications in the glycosidic ring and the R_1

substituent at the phenyl ring should improve ligand binding. Additionally, despite their lower activity, monosubstituted triazoles showed a similar binding mode of known active azoles and could be used as a starting point in the design of new ligands.

ACKNOWLEDGMENTS

The authors acknowledge the PROPP/UFOP, FAPEMIG (APQ-00820-19), and CNPq agencies for the scholarships and financial support provided. The authors acknowledge the "Laboratório Multiusuário de Caracterização de Moléculas (Pharmacy School at the Federal University of Ouro Preto)" for nuclear magnetic resonance analysis. The authors acknowledge the "Base de Estruturas Cristalinas/CAPES (Crystalline Structures Base)" for the GOLD software licensing. The authors would also like to acknowledge the "Laboratório Multiusuário de Proteômica e Biomoléculas (LMU-ProtBio), do Núcleo de Pesquisas em Ciências Biológicas" (from the Research Nucleus in Biological Sciences), Federal University of Ouro Preto, MG, Brazil, for providing the required equipments and technical expertise for the sample processing and analyses.

CONFLICT OF INTEREST

The authors declare no conflict of interest.

DATA AVAILABILITY STATEMENT

Data sharing is not applicable to this article as all data have been made available in the "Supplementary Material" section.

ORCID

Diogo Teixeira Carvalho https://orcid.org/0000-0002-6362-2822
Danielle Ferreira Dias https://orcid.org/0000-0001-9129-4734
Thiago Belarmino de Souza https://orcid.org/0000-0003-3627-6407

REFERENCES

Achard, T., Lepronier, A., Gimbert, Y., Clavier, H., Giordano, L., Tenaglia, A., & Buono, G. (2011). A regio- and diastereoselective platinum-catalyzed tandem [2+1]/[3+2] cycloaddition sequence. *Angewandte Chemie*, *123*, 3614–3618. https://doi.org/10.1002/ange.201007992

Alonso, H., Bliznyuk, A. A., & Gready, J. E. (2006). Combining docking and molecular dynamic simulations in drug design. *Medicinal Research Reviews*, *26*, 531–568. https://doi.org/10.1002/med.20067

Balogh, M. P. (2004). Debating resolution and mass accuracy in mass spectrometry. *Spectroscopy*, *19*, 34–40.

Banert, K., Hagedorn, M., Hemeltjen, C., Ihle, A., Weigand, K., & Priebe, H. (2016). Synthesis of *N*-unsubstituted 1,2,3-triazoles via a cascade including propargyl azides, allenyl azides, and triazafulvenes. *Arkivoc*, *1*, 338–361. https://doi.org/10.24820/ark.5550190.p009.846

Bhattacharya, S., Sae-Tia, S., & Fries, B. C. (2020). Candidiasis and mechanisms of antifungal resistance. *Antibiotics*, *9*, 1–19. https://doi.org/10.3390/antibiotics9060312

EUCAST - European Committee on Antibiotic Susceptibility Testing. (2008). *Method for the determination of minimum inhibitory concentration (mic) by broth dilution of fermentative yeasts*. Definitive document E.Def. 7.2, European Society of Clinical Microbiology and Infectious Diseases, 2008.

Guilherme, F. D., Simonetti, J. E., Foolquitto, L. R. S., Reis, A. C. C., Oliver, J. C., Dias, A. L. T., Dias, D. F., Carvalho, D. T., Brandão, G. C., & Souza, T. B. (2019). Synthesis, chemical characterization and antimicrobial activity of new acylhydrazones derived from carbohydrates. *Journal of Molecular Structure*, *1184*, 349–356.

Hargrove, T. Y., Friggeri, L., Wawrzak, Z., Qi, A., Hoekstra, W. J., Schotzinger, R. J., York, J. D., Peter Guengerich, F., & Lepesheva, G. I. (2017). Structural analyses of *Candida albicans* sterol 14α-demethylase complexed with azole drugs address the molecular basis of azole-mediated inhibition of fungal sterol biosynthesis. *Journal of Biological Chemistry*, *292*, 6728–6743. https://doi.org/10.1074/jbc.M117.778308

Kirton, S. B., Murray, C. W., Verdonk, M. L., & Taylor, R. D. (2005). Prediction of binding modes for ligands in the cytochromes P450 and other heme-containing proteins. *Proteins: Structure, Function, and Bioinformatics*, *58*, 836–844. https://doi.org/10.1002/prot.20389

Lemkul, J. (2019). From proteins to perturbed hamiltonians: A suite of tutorials for the GROMACS-2018 molecular simulation package [Article v1.0]. *Living Journal of Computational Molecular Science*, *1*, 1–53. https://doi.org/10.33011/livecoms.1.1.5068

Lepesheva, G. I., Friggeri, L., & Waterman, M. R. (2018). CYP51 as drug targets for fungi and protozoan parasites: Past, present and future. *Parasitology*, *145*, 1820–1836. https://doi.org/10.1017/S0031182018000562

Lepesheva, G. I., & Waterman, M. R. (2004). CYP51 - The omnipotent P450. *Molecular and Cellular Endocrinology*, *215*, 165–170. https://doi.org/10.1016/j.mce.2003.11.016

Mani Chandrika, K. V. S., & Sharma, S. (2020). Promising antifungal agents: A minireview. *Bioorganic & Medicinal Chemistry*, *28*, 115398. https://doi.org/10.1016/j.bmc.2020.115398

Monk, B. C., Tomasiak, T. M., Keniya, M. V., Huschmann, F. U., Tyndall, J. D. A., O'Connell, J. D., Cannon, R. D., McDonald, J. G., Rodriguez, A., Finer-Moore, J. S., & Stroud, R. M. (2014). Architecture of a single membrane spanning cytochrome P450 suggests constraints that orient the catalytic domain relative to a bilayer. *Proceedings of the National Academy of Sciences*, *111*, 3865–3870. https://doi.org/10.1073/pnas.1324245111

Mosmann, T. (1983). Rapid colorimetric assay for cellular growth and survival: Application to proliferation and cytotoxicity assays. *Journal of Immunological Methods*, *65*, 55–63.

Peyton, L. R., Gallagher, S., & Hashemzadeh, M. (2015). Triazole antifungals: A review. *Drugs of Today*, *51*, 705–718. https://doi.org/10.1358/dot.2015.51.12.2421058

Pote, A. R., Vannam, R., Richard, A., Gascón, J., & Peczuh, M. W. (2018). Formation of and glycosylation with per-O-acetyl septanosyl halides: rationalizing somplex reactivity en route to p-nitrophenyl septanosides. *European Journal of Medicinal Chemistry*, *14*, 1709–1719. https://doi.org/10.1002/ejoc.201800310

Revie, N. M., Iyer, K. R., Robbins, N., & Cowen, L. E. (2018). Antifungal drug resistance: Evolution, mechanisms and impact. *Current Opinion in Microbiology*, *45*, 70–76. https://doi.org/10.1016/j.mib.2018.02.005

Safavi, M., Asthari, A., Khalili, F., Mirfazli, S. S., Saeedi, M., Ardestani, S. K., Ranjbar, P. R., Tehrani, M. B., Larijani, B., & Mahdavi, M. (2019). Novel quinazolin-4(3H)-one linked to 1,2,3-triazoles: Synthesis and anticancer activity. *Chemical Biology & Drug Design*, *92*, 1373–1381. https://doi.org/10.1111/cbdd.13203

Souza, T. B., Brito, K. M. O., Silva, N. C., Rocha, R. P., Sousa, G. F., Duarte, L. P., Coelho, L. F. L., Dias, A. L. T., Veloso, M. P., Carvalho, D. T., & Dias, D. F. (2016). New eugenol glucoside-based rerivative shows fungistatic and fungicidal activity against opportunistic *Candida glabrata*. *Chemical Biology & Drug Design*, *87*, 83–90.

Souza, T. B., Orlandi, M., Coelho, L. F. L., Malaquias, L. C. C., Dias, A. L. T., Carvalho, R. R., Silva, N. C., & Carvalho, D. T. (2014). Synthesis and in vitro evaluation of antifungal and cytotoxic activities of eugenol glycosides. *Medicinal Chemistry Research*, *23*, 496–502. https://doi.org/10.1007/s00044-013-0669-2.

Strickland, A. B., & Shi, M. (2021). Mechanisms of fungal dissemination. *Cellular and Molecular Life Sciences*, *78*, 3219–3238. https://doi.org/10.1007/s00018-020-03736-z

Twentyman, P. R., & Luscombe, M. (1987). A study of some variables in a tetrazolium dye (MTT) based assay for cell growth and chemosensitivity. *British Journal of Cancer*, *56*, 279–285. https://doi.org/10.1038/bjc.1987.190

Whaley, S. G., Berkow, E. L., Rybak, J. M., Nishimoto, A. T., Barker, K. S., & Rogers, P. D. (2017). Azole antifungal resistance in *Candida albicans* and emerging non-albicans *Candida* species. *Frontiers in Microbiology*, *7*, 1–7. https://doi.org/10.3389/fmicb.2016.02173

SUPPORTING INFORMATION

Additional supporting information may be found online in the Supporting Information section.

How to cite this article: Magalhães, L. S. D., Reis, A. C. C., Nakao, I. A., Péret, V. A. C., Reis, R. C. F. M., Silva, N. C., Dias, A. L. T., Carvalho, D. T., Dias, D. F., Brandão, G. C., Braga, S. F. P., & Souza, T. B. D. (2021). Glucosyl-1,2,3-triazoles derived from eugenol and analogues: Synthesis, anti-*Candida* activity, and molecular modeling studies in CYP-51. *Chemical Biology & Drug Design*, 00, 1–11. https://doi.org/10.1111/cbdd.13948